

## Role of Transport and MHD Stability in Simulations of H-mode Pedestal Development in ELMy Plasmas

A.Y. Pankin 1), G.Y. Park 2), J. Cummings 3), C.S. Chang 2,4), G. Bateman 1), D. Bunner 5), R.J. Groebner 6), J.W. Hughes 5), B. LaBombard 5), J.L. Terry 5), A.H. Kritz 1), S. Ku 3), T. Rafiq 1), and P.B. Snyder 6)

1) Lehigh University, Bethlehem, PA, USA

2) New York University, New York, NY, USA

3) Caltech, Pasadena, CA, USA

4) Korea Advanced Institute of Science and Technology, Daejeon, Korea

5) MIT Plasma Science and Fusion Center, Cambridge, MA, USA

6) General Atomics, San Diego, CA, USA

E-mail: [pankin@lehigh.edu](mailto:pankin@lehigh.edu)

**Abstract.** This study addresses the development of a scaling of the H-mode pedestal in tokamak plasmas with type I ELMs. In particular, the scaling studies carried out illustrate the dependence of the pedestal properties and the resulting divertor heat load width as a function of plasma elongation and plasma current. H-mode pedestal profiles for DIII-D and Alcator C-Mod tokamaks are considered: DIII-D for low B-field, low-density, high temperature plasmas; and Alcator C-Mod for a high B-field, high-density plasmas. The simulations in this study use realistic diverted geometry and are self-consistent with the inclusion of kinetic neoclassical physics, theory-based anomalous transport models with the  $\mathbf{E} \times \mathbf{B}$  flow shearing effects, as well as an MHD ELM triggering criterion. Scalings for the pedestal width and height are developed as a function of the scanned plasma parameters. Differences in the electron and ion temperature pedestal scaling are investigated. The neoclassical divertor heat load fluxes are computed with the XGC0 code and a relation for the dependence of the divertor heat load width on the plasma current is derived. In the development of this relationship, effects of neutral collisions and anomalous transport are taken into account. Changes in the neoclassical divertor heat load fluxes associated with the introduction of the neutral collision and anomalous transport effects are described.

### 1. Introduction

The XGC0 kinetic guiding-center code [1] is used to investigate the basic kinetic neoclassical behavior of tokamaks with a realistic divertor geometry. For the anomalous transport, a radial random-walk is superposed in the Lagrangian neoclassical particle motion, using the FMCFM interface to the theory-based MMM95 and GLF23 models. These anomalous models include transport driven by drift-wave instabilities, such as the electron and ion temperature gradient driven modes and trapped electron modes. The MMM95 model includes a resistive ballooning component that is particularly important near the plasma edge. The sheared  $\mathbf{E} \times \mathbf{B}$  flows result in a reduction of anomalous transport, which could lead to the formation of an edge transport barrier and the transition to the H-mode improved confinement in tokamaks. The effect of  $\mathbf{E} \times \mathbf{B}$  flow shear quenching is implemented through a flow shear suppression factor [2-4]:  $F_s = 1 / (1 + (\tau_c \omega_{\mathbf{E} \times \mathbf{B}})^2)$ , where  $\tau_c$  is the correlation time of fluctuations for the case without flow and  $\omega_{\mathbf{E} \times \mathbf{B}}$  is the normalized  $\mathbf{E} \times \mathbf{B}$  flow shear rate:  $\omega_{\mathbf{E} \times \mathbf{B}} = |R B_\theta / B_\phi \partial / \partial r (E_r / R B_\theta)|$ . Growth of the pedestal by neutral penetration and ionization is limited by an ELM instability criterion computed by the ELITE MHD stability code [5]. XGC0 and ELITE coupling is automated in the EFFIS computer science framework.

## 2. H-Mode Pedestal Width and Height Dependence on the Elongation and Triangularity

The study of DIII-D discharges includes a scan with respect to plasma shaping. Three DIII-D discharges are analyzed in this section. The DIII-D discharge 136674 has high elongation,  $\kappa \approx 1.7$ , which is typical for most DIII-D discharges, but rather low triangularity  $\delta \approx 0.1$ . The DIII-D discharge 136693 has almost circular geometry with the elongation  $\kappa \approx 1.2$  and triangularity  $\delta \approx 0.03$ . The third DIII-D discharge studied in this section, DIII-D discharge 136705, has very small elongation,  $\kappa \approx 1.3$ , but relatively high triangularity,  $\delta \approx 0.3$ . Thus, the elongation is being varied by a factor of 1.4 and the triangularity is being varied by a factor of 10 in this study.

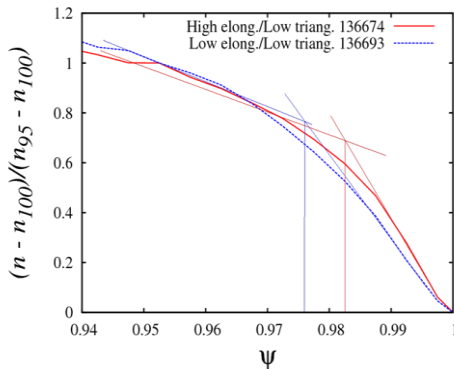


Fig. 1: Normalized plasma density profiles as a function of normalized poloidal flux for DIII-D discharges with different elongations and similar triangularities. Here,  $n_{100}$  and  $n_{95}$  are the plasma densities at the separatrix and at 95% of the normalized poloidal flux, respectively.

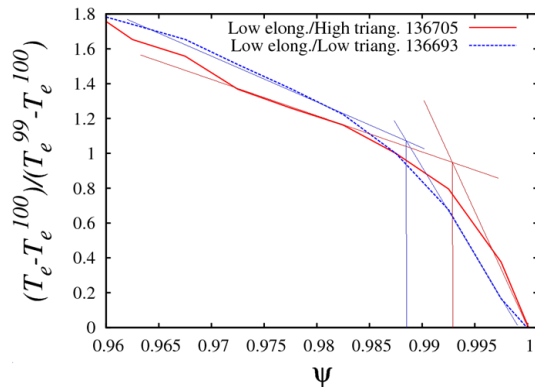


Fig. 2: Normalized electron temperature profiles as a function of normalized poloidal flux for DIII-D discharges with different triangularities and similar elongations. Here,  $T_e^{100}$  and  $T_e^{99}$  are the electron temperatures at the separatrix and at 98.8% of the normalized poloidal flux, respectively.

These simulations do not include the effects associated with the anomalous transport. The anomalous transport was selected at small residual level through the whole edge region for all DIII-D discharges that are investigated in this section. The electron and ion thermal diffusivity have been selected to be  $0.02 \text{ m}^2/\text{sec}$  in the pedestal region and  $0.4 \text{ m}^2/\text{sec}$  in the SOL region and the particle diffusivity has been selected to be  $0.01 \text{ m}^2/\text{sec}$  in the pedestal region and  $0.05 \text{ m}^2/\text{sec}$  in the SOL region. The motivation of the selection of anomalous transport coefficients at a small residual level is that the focus of this study is the neoclassical and MHD effects on the H-mode pedestal structure. However, a residual anomalous transport was still necessary in these simulations. Without the anomalous transport, the plasma density becomes too low in the near outer separatrix region. The plasma density depletion leads to unrealistic ion and electron temperature profiles. These changes to the plasma profiles might occur before the H-mode pedestal develops enough to trigger the peeling or ballooning instabilities that would lead to an ELM crash.

The simulation results illustrate a scaling that is qualitatively similar to some experimental observations. Fig. 1 shows the normalized plasma density profiles as a function of the normalized poloidal flux for high and low elongation DIII-D discharges. Fig. 2 shows the normalized electron temperature profiles for low and high triangularity DIII-D discharges. In XGC-0 kinetic simulations, it has been found that the pedestal width is smaller for high elongation and high triangularity discharges. In the discharges considered in this study, the effect

of increased elongation manifests itself in the plasma density profiles first, while the effect of increased triangularity manifests itself in the electron temperature profiles first. It has also been found that the pedestal width for the ion temperature profile is much wider than the pedestal width for the electron temperature and plasma density profiles. The pedestal height is found to be significantly larger in the discharges with larger elongation.

While the neoclassical effect together with the MHD stability conditions that are verified using the ideal stability ELITE code can explain some experimental trends, the question about the contributions of the anomalous transport in the pedestal and SOL regions remains. This question will be partially addressed in the next section.

### 3. Study of the effects associated with the anomalous transport

The anomalous transport in the plasma edge region has been previously analyzed in a number of studies. In particular, it has been pointed out that particle pinches might play an important role in the pedestal region [6]. Experimental observations and some analytical models suggest that anomalous transport in SOL can be significantly larger than in the pedestal region and

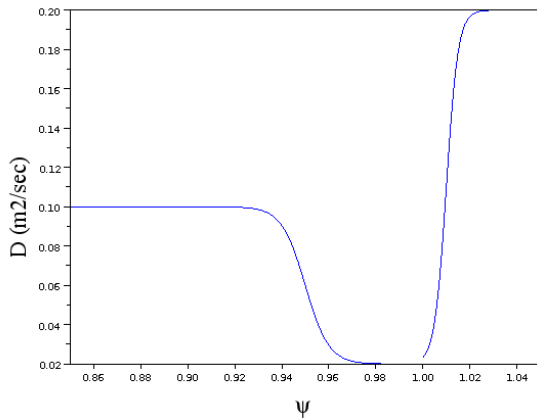


*Fig. 3: Typical particle diffusivity profile that is used in the modeling with the XGC0 code.*

intermittent. Studies of the anomalous transport in the plasma edge region are typically based on the analysis of experimental data that should include a robust model for the neoclassical transport. Particle and thermal fluxes obtained from analysis of experimental data include contributions from both the anomalous and neoclassical transport so that the neoclassical transport needs to be deducted to get the correct anomalous fluxes and effective diffusivities. Effects associated with neutral collisions and recycling are other factors that can affect the total particle fluxes and

should be carefully taken into consideration.

The kinetic XGC0 code is designed for the first-principle neoclassical computations and includes several advanced models for neutral collisions including the DEGAS2 model. Also, the XGC0 code takes into consideration the recycling and other particle effects that contribute to the total particle fluxes. Thus, the XGC0 code can be used for the analysis of experimental fluxes in order to derive the effective diffusivities. These anomalous effective diffusivities can be also used for comparisons with the analytical models for anomalous transport. In particular, it is important to understand the origin of particle and thermal pinches in the pedestal region. While the origin of particle and thermal pinches is not studied in this work, it is worth mentioning that there are several physical effects that can be associated with the pinches in the pedestal area such as curvature effects and parallel compression.

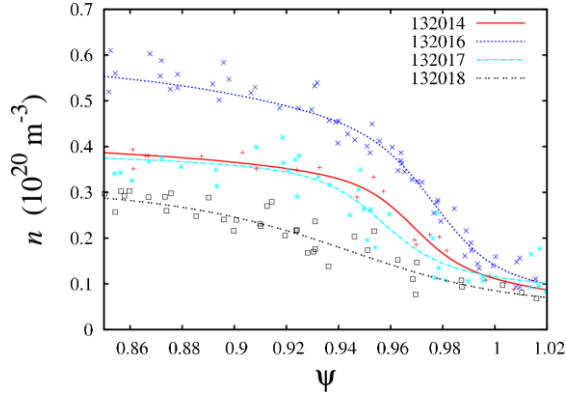


Fig. 4: Plasma density profiles in the DIII-D discharges that represent plasma current scan. The experimental data are shown as dots and fitted profiles are shown as solid and dashed curves.

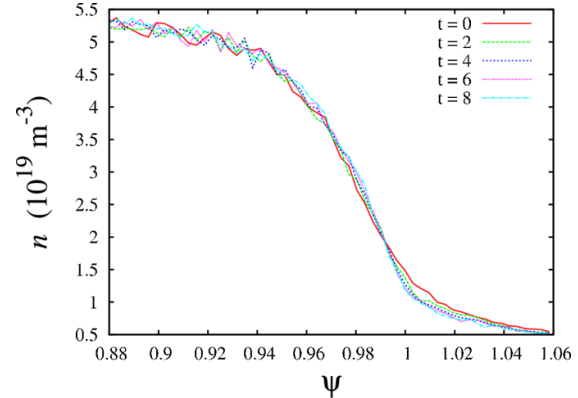


Fig. 5: Simulation results of the plasma density profile in the DIII-D discharge 132016 for the first eight ion transit periods. The experimental plasma density profile is shown in red.

The purpose of the study described in this section is to derive the anomalous effective diffusivities that can reproduce the experimental profiles when they are used in the neoclassical kinetic XGC0 code. These profiles will be used in the next section of this paper for the computation of the divertor heat load fluxes. The effective diffusivities are selected in the form that is given by Fig. 3. There are three regions of constant diffusivities that are separated by two narrow transitional regions that use *tanh*-fit. The levels of anomalous transport in all three regions, locations of transitional regions and their widths are adjustable parameters. The profiles for the particle diffusivities as well as for the electron and ion thermal diffusivities are independent from each other. These profiles are adjusted to find a steady state solution that reproduces the experimental profiles.

A series of four DIII-D discharges that represent plasma current scan [7] is analyzed in this study. In this series of DIII-D discharges, the total plasma current is varied from 0.51 to 1.50 MA with an approximately fixed toroidal magnetic field ( $B_T \approx 2.1$  T), plasma shape ( $\delta \approx 0.55$ ), and normalized toroidal beta ( $\beta_n \approx 2.1$ -2.4). The discharges differ by total plasma current, auxiliary heating power, and plasma densities that are given in Table 1 and Fig. 4 correspondingly.

Discharge #	EFIT time, msec	Plasma current, MA	Auxiliary heating power, MW
132016	3023	1.50	8.12
132014	3023	1.17	7.36
132017	2998	0.85	8.50
132018	1948	0.51	7.10

Table 1. DIII-D discharges analyzed in this study and their parameters.

The anomalous diffusivity profiles are selected so that the resulting profiles remains close to the experimental profiles at least up to eight ion transit periods (see Fig. 5).

There is a clear evidence of strong pinches in the particle and thermal channels of anomalous transport. While the mechanisms that result in these pinches are not the subject of this study, we have analyzed the anomalous transport in the DIII-D discharges, which are described in Table 1, with the drift wave anomalous transport model MMM95 that is implemented in the XGC0 code. It has been found that the most contribution to the anomalous transport in the outer pedestal region comes from the turbulence driven by the resistive-ballooning instabilities (see Fig. 6). The resistive-ballooning model gives somewhat larger contribution for the lower plasma current and lower plasma density discharges 132017 and 132018 comparing to the contributions to the anomalous transport for the higher plasma current and higher density discharges 132014 and 132016.

There are no physical effects in the resistive-ballooning model that can explain the particle and thermal pinches that are found to be important in the analyzed discharges. As result, the effective diffusivities computed with the MMM95 model are found to be overpredicted and the corresponding plasma profiles are found to be under-predicted compared to the experimental profiles and profiles computed with the diffusivities derived in the analysis mode. The computations of the divertor heat fluxes that are presented in the next section of this report use the diffusivities obtained in the analysis mode. It should be pointed that the theory-based reduced model for the resistive-ballooning modes might need a significant revision that would extend its validity to the SOL and near separatrix regions.

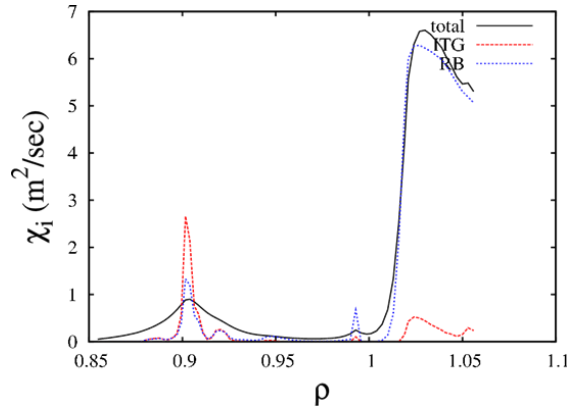


Fig. 6: Ion thermal diffusivity profiles predicted with drift-wave transport model MMM95 for the DIII-D discharge 132016 at five ion transit periods. The contribution from anomalous transport driven by ion-temperature gradient (ITG) modes is shown in red. The contribution from anomalous thermal diffusivity driven by resistive ballooning modes is shown in blue. The smoothed total ion thermal diffusivity that is used in the XGC0 simulations is shown in black.

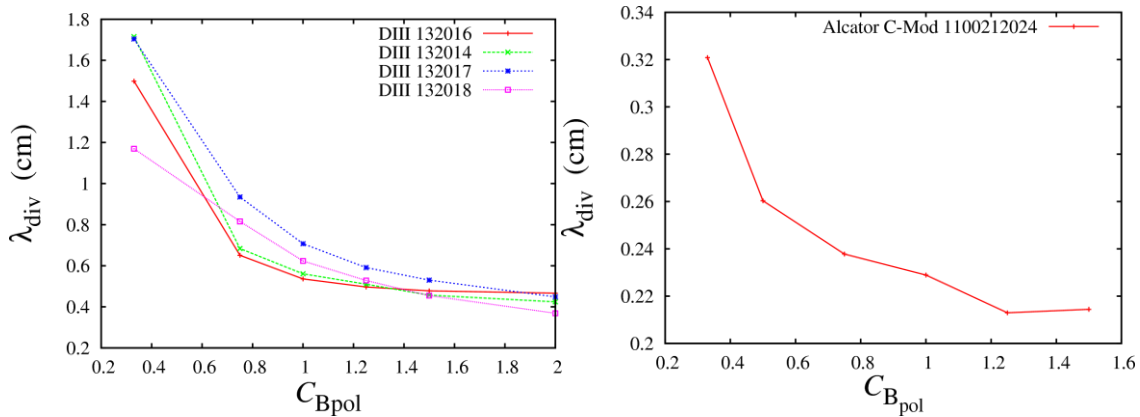


Fig. 7: The divertor heat load widths for four DIII-D discharges (first panel) and one Alcator C-Mod discharge (second panel) as functions of poloidal magnetic field scaling factor.

#### 4. Divertor heat load studies for the DIII-D and Alcator C-Mod tokamaks

Understanding physical effects that contribute to divertor heat load fluxes is important for experiment planning, design of future tokamaks, and development of new models for the SOL region. In this study, the neoclassical effects and effects related to neutral collisions and anomalous transport are investigated. Four DIII-D discharges described in Table 1 are analyzed here. In addition, one Alcator C-Mod discharge 1100212024 that was a part of Alcator C-Mod/DIII-D similarity campaign is analyzed. The divertor heat load widths,  $\lambda_{div} \equiv \int q_{\parallel} d\rho / q_{\parallel}^{max}$ , for four DIII-D discharges and one Alcator C-Mod discharge as functions of the poloidal magnetic field amplification factor  $C_{Bp}$  are shown on Fig. 7. This scaling factor is an internal numerical multiplier introduced in the XGC0 code in order to alter the initial equilibrium by scaling the poloidal flux. If the toroidal flux is not modified,  $I_{pi} \propto B_p \propto \partial\psi/\partial\rho$ , where  $\psi$  is the normalized poloidal flux. Thus, the amplification factor  $C_{Bp}$  can be also considered as a scaling factor for the total plasma current  $I_{pl}$ . The neoclassical divertor heat load width in the Alcator C-Mod discharge is found to be approximately 2.3 mm, which is about 40% below the experimentally observed value of 3.13 mm in the base case ( $C_{Bp}=1$ ) [8]. As it will be shown below, the anomalous effects typically increase the divertor heat load width bringing the simulation results and experimental data closer to each other. It has been found that the neoclassical heat load width for all four DIII-D discharges follows approximately the  $1/I_p$  dependence. There is neither anomalous transport nor neutral effects included in these simulations. The difference in the slopes of the predicted divertor heat load widths vs  $C_{Bp}$  for different DIII-D discharges might be attributed to different collisionality in these discharges. The differences in slopes are especially noticeable if two set of discharges with lower (DIII-D discharges 132017 and 132018) and higher plasma densities (DIII-D discharges 132014 and 132016) are compared. This computational result on the effect of collisionality on divertor heat fluxes still needs to be confirmed in further computational and analytical analysis. In the meantime, there is no doubt that the neoclassical divertor heat load width is decreasing with increasing plasma current for all DIII-D discharges studied in this research. Correlation between the divertor heat load width and the width of radial electric field profiles in the pedestal region is found. The width of radial electric field profiles is reduced with increased plasma current. Fig. 8 shows the radial electric field profiles for low and high plasma current DIII-D discharges 132016 and 132018. The width of radial electric

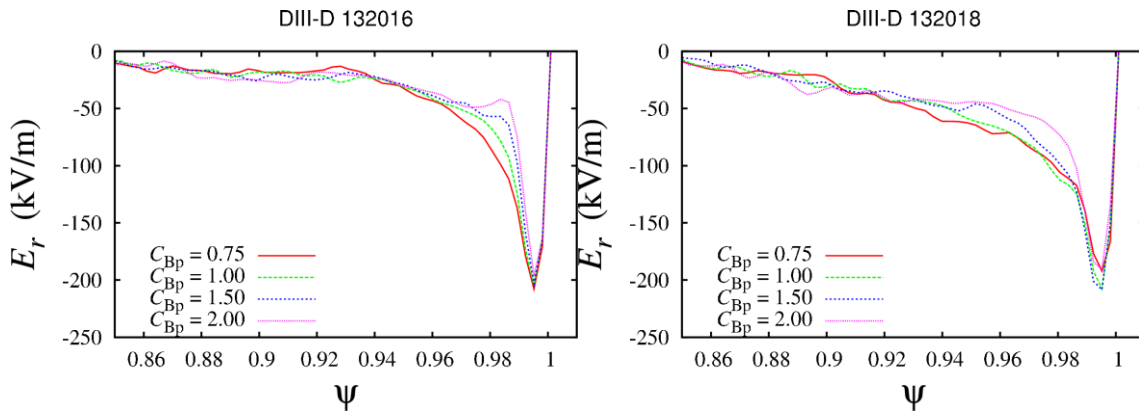


Fig. 8: The radial electric field profiles in low and high plasma current DIII-D discharges 132016 and 132018 for different values of plasma current scaling factor  $C_{Bp}$ .

field profiles in the H-mode pedestal region reduces when the plasma current scaling factor  $C_{Bp}$  is increased.

Simulation results that are shown on Fig. 9 demonstrate the effects of neutral collisions and anomalous transport. The dependence of the divertor heat load width is weakly affected by neutral collisions, but it can be completely modified when the anomalous transport is introduced and is applied uniformly for all poloidal angles. Changes to the divertor heat load width scaling related to the ballooning nature of resistive-ballooning modes, that are likely to be major players in the region near the separatrix, are shown as purple curve on Fig. 9. In these simulations, the anomalous transport is applied in the region within  $45^\circ$  from the midplane. The neoclassical dependence of the divertor heat load width on the total plasma current is preserved for the high-density DIII-D discharge 132016 and almost vanished for the low-density DIII-D discharge 132018 (not shown on Fig. 9). The dependence of divertor heat load width on the current density was weakest for the DIII-D discharge 132018 among discharges studied in this research (see Fig. 7). The introduction of anomalous transport effects typically widens the divertor heat load width. This observation becomes evident, when red and purple plots on Fig. 9 are compared.

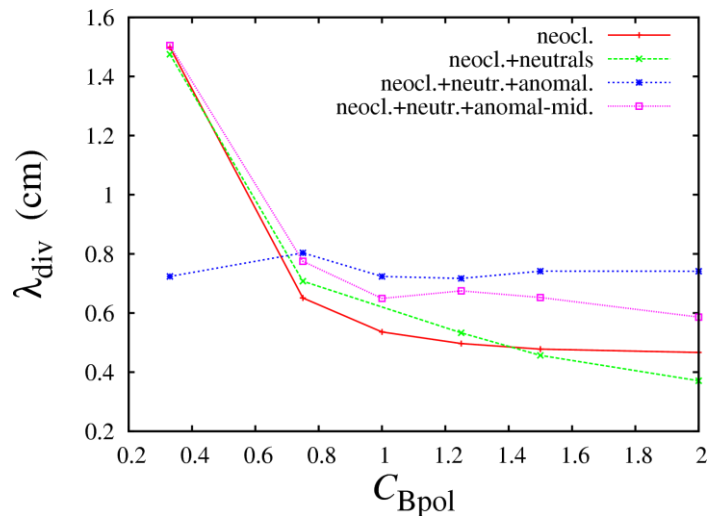


Fig. 9: Effects of neutral collisions and anomalous transport on the divertor heat load width scaling in the XGC0 simulations of the DIII-D discharge 132016. The red curve shows the neoclassical scaling that does not include the effects of neutral collision and anomalous transport. The green curve shows the effect of neutral collisions. The anomalous transport that is applied uniformly for all poloidal angles in used in the simulations resulted in the blue curve. The purple curve shows the divertor heat load width scaling when the anomalous transport is applied within  $45^\circ$  from the midplane.

## 5. Conclusions

The dependence of H-mode pedestal width and height on plasma shaping is investigated in coupled XGC0-ELITE simulations. The initial plasma profiles from equilibria reconstructed from three DIII-D experiments, where the elongation and triangularity have been significantly varied, are evolved in the kinetic neoclassical XGC0 code. As plasma profiles evolve, the ideal MHD stability ELITE code is used to check if peeling-ballooning stability conditions are violated. These conditions set maximum H-mode pedestal height. In this research, it has been found that the neoclassical effects and MHD stability conditions alone can explain some experimentally observed trends. In particular, it has been found that the pedestal height is the largest in the DIII-D discharges with the largest elongation. The effect of triangularity is found to be somewhat weaker comparing to the effect of elongation. As a result, it might be more difficult to reach a specific pedestal height and width by altering the triangularity and keeping the elongation fixed. It has been also found that the H-mode pedestal width for electron temperature and plasma density is affected differently by elongation and triangularity.

The effect of elongation reveals itself on the plasma density profiles first, while the effect of triangularity reveals itself on the electron temperature profiles first. Pedestal width for the plasma density profiles decreases with the elongation and is almost independent of triangularity, while the pedestal width for the electron temperature profiles decreases with the triangularity and is almost independent of elongation. It should be pointed out that these conclusions might change if the anomalous transport is included in this analysis. The theory-based MMM95 model has been tested for several DIII-D discharges that represent plasma current scan. The anomalous transport driven by the resistive ballooning modes is found to be one of the major contributors to the total anomalous transport in the near separatrix region. However, it is also found that the resistive-ballooning component of MMM95 produces too much transport if compared with effective diffusivities computed in the analysis mode using the XGC0 code. In addition, there are strong indications of particle and thermal pinches in the pedestal regions of Alcator C-Mod and DIII-D discharges, while the resistive-ballooning model does not predict particle and thermal pinches in these plasma regions. There is an urgent need for an improved resistive-ballooning model that can be applied for predictive modeling in the H-mode pedestal and SOL regions.

The neoclassical scaling of divertor heat load width with the plasma in DIII-D and Alcator C-Mod discharges is studied in this report. It has been found that the divertor heat load width is broader for lower plasma currents for all discharges simulated in this work. The Alcator C-Mod discharge has weaker scaling of the width of the divertor heat load with the plasma current relative to the four DIII-D discharges that were analyzed in this study. This trend reproduces the experimental observations [8, 9]. The differences in neoclassical scaling of divertor heat load width might be attributed to difference in collisionality in Alcator C-Mod and DIII-D discharges. This hypothesis will be verified in future studies with the XGC0 code. The effect of neutral collisions does not significantly modify this dependence, while the inclusion of anomalous transport typically widens the divertor heat load width and enhances the heat load fluxes on the divertor.

- [1] C.S. CHANG *et al.*, Phys. Plasmas **11** (2004) 2649.
- [2] S. HAMAGUCHI and W. HORTON, Phys. Fluids **B 4** (1992) 319.
- [3] T.S. HAHM and K.H. BURRELL, Phys. Plasmas **2** (1995) 1648.
- [4] K.H. BURRELL, Phys. Plasmas **4** (1997) 1499.
- [5] P.B. SNYDER *et al.*, Phys. Plasmas **9** (2002) 2037.
- [6] W.M. STACEY, Phys. Plasmas **17** (2010) 052506.
- [7] R. GROEBNER *et al.*, Nucl. Fusion **49** (2009) 085037.
- [8] B. LABOMBARD *et al.*, J. Nucl. Materials (in press).
- [9] C.J. LASNIER *et al.*, Nucl. Fusion **38** (1998) 1225; D.N. HILL *et al.*, J. Nucl. Materials **196-198** (1992) 204; C.J. LASNIER *et al.*, Proc. of 36th EPS Conference (Sofia, Bulgaria, 2009).

---

<sup>§</sup> This work supported by the U.S. Department of Energy under DE-SC0000692, DE-FC02-08ER54985, DE-FG02-06ER54845, DE-FG02-92ER54141, DE-FG03-98ER54461, DE-FG02-94ER54084, DE-FC02-04ER54698, DE-FC02-99ER54512.